Effects of Temperature on Surface-Controlled Dislocation Multiplication in Body-Centered-Cubic Metal Nanowires

Gyuho Song*, Seok-Woo Lee

Department of Materials Science and Engineering & Institute of Materials Science, University of Connecticut, 97 North Eagleville Road, Unit 3136, Storrs CT 06269-3136, USA

*Corresponding author.

E-mail address: gyuho.song@uconn.edu (Gyuho Song)

Abstract:

Recent computational studies revealed that screw dislocations in body-centered-cubic (bcc) metal nanowires can self-multiply through cross-slip near the free surface. This unique process was termed surface-controlled dislocation multiplication (SCDM). In bcc metals, screw dislocation motion and its cross-slip behavior are often related to thermally activated processes; due to this relation, SCDM is expected to be highly temperature-sensitive. In this study, therefore, we investigated how temperature influences the SCDM in bcc molybdenum and niobium nanowires using atomistic simulations. Regardless of the difference in lattice resistance at a given temperature, both systems show similar trends of critical shear stress of SCDM with respect to temperature. The temperature dependence was found to be divided into three different regimes; (1) lattice-resistance-dominant; (2) segmentation-dominant; (3) steady-state segmentation. The presence of these three regimes will be discussed in terms of the temperature-dependence of the lattice resistance and the dynamics of dislocation segmentation in the nano-scale volume. Our results provide a fundamental understanding of screw dislocation behavior in bcc metals at the nanometer scale and varying temperatures.

Keywords: Crystal plasticity, Molecular dynamics, Screw dislocation multiplication, Bcc metal

(Some figures may appear in color in the online journal)

1. Introduction

Mechanical properties of metals are mostly controlled by the motion of dislocations, which is a line imperfection in crystalline solids. Thus, the understanding of dislocation behavior is critical to develop structurally robust metallic components in devices [1, 2]. Recently, nano-/micro-electro-mechanical systems (NEMS/MEMS) have been developed to produce small-scale sensors and actuators. It is necessary to understand how dislocations behave in the nanoscale volume in order to make mechanically-reliable miniaturized systems [3-5]. For the last two decades, nanomechanical testing techniques have been extensively developed to study dislocation plasticity in small metals such as thin films, micropillars, nanowires, and nanoparticles [6-12]. These works have demonstrated the presence of strong size effects on mechanical properties when a sample dimension reaches microstructural length scales. In the case of a single-crystalline metal, the interaction between dislocations and free surface leads to size-affected strength, scale-free intermittency, dislocation starvation, Schmidt's law breakdown, and so forth [13-15].

Recent experimental studies demonstrated that body-centered-cubic (bcc) metallic nanopillars exhibit significant dislocation multiplication while face-centered-cubic (fcc) metallic nanopillars do not. Bei *et al*. found that dislocation-free bcc Mo-alloy single-crystal nanopillars are catastrophically strain-softened, presumably by nucleation of dislocations followed by their extensive multiplication [16]. Chisholm *et al.* observed extremely high dislocation density right after yielding in bcc Mo-alloy nanofibers through *in-situ* transmission electron microscope (TEM) nanomechanical tests [17]. Furthermore, Brinckmann *et al.* showed that the stress-strain curves of bcc nanopillars are usually much smoother than those of fcc nanopillars [18]. Their post-mortem TEM analysis revealed higher dislocation density in bcc nanopillars while fcc nanopillars are nearly dislocation-free even after applying significant plastic deformation. All this experimental

evidence indicates that bcc metals are able to induce significant dislocation multiplication in the nanoscale volume.

To clarify the mechanism of dislocation multiplication which occurs preferentially in bcc metal nanopillars, Weinberger *et al.* performed both dislocation dynamics (DD) and molecular dynamics (MD) simulations on bcc molybdenum nanowires containing a single screw dislocation [19]. It was discovered that a screw dislocation can self-multiply through cross-slips near the free surface, which is followed by the formation and operation of dynamic dislocation sources. Strong image stresses force both ends of the screw dislocation to cross-slip from {1 1 0} to {1 1 2} planes, creating two dynamic single arm dislocation sources joined at a mobile pinning point. If the applied stress is higher than a critical stress, these two dynamic dislocation sources can produce new dislocations. Weinberger *et al.* termed this phenomenon surface-controlled dislocation multiplication (SCDM) [19]. Their computational studies showed that the critical stress of SCDM is a strong function of pillar diameter. They also confirmed that SCDM cannot be seen easily in fcc nanowires, particularly for low stacking fault energy materials such as gold, because the wide width of dislocation core does not permit a cross-slip at the free surface, which is a prerequisite process for SCDM.

Nowadays, studies on small-scale mechanical properties of materials under harsh environments have drawn increased attention due to the necessity to develop micro-/nano-scale devices working in different chemical and thermal environments [20, 21]. MEMS/NEMSs which operate in the presence of high temperature, corrosive media and/or high radiation can reduce weight, improve machine reliability, and reduce cost in strategic market sectors such as automotive, avionics, oil well logging, nuclear power, and space exploration [22-24]. In order to produce a mechanically-reliable small-scale device used in various environments, it is important to

understand how environmental conditions influence dislocation behaviors at the micro-/nano-meter length scales. Note that the motion of dislocations in bcc metals is strongly affected by temperature [25]. Particularly for a screw dislocation, the double-kink mechanism, which is a thermally-activated process, controls its mobility. Furthermore, cross-slip of screw dislocations is usually regarded as a thermally-activated process. At an elevated temperature, strong thermal vibrations would induce cross-slip more frequently and could lead to different evolutions of the dislocation structure. Therefore, SCDM of a screw dislocation in bcc nanowires, which requires cross-slip at the free surface, could be significantly sensitive to temperature.

In this work, therefore, we performed atomistic simulations on two representative bcc metals, molybdenum (Mo) and niobium (Nb) nanowires containing a single screw dislocation to study the effects of temperature on SCDM. We developed the constant uniaxial stress method and characterized the critical shear stress ($\tau_{[111](1\bar{2}1)}$) of SCDM as a function of temperature. Both systems showed three distinct regimes of the critical shear stress of SCDM with respect to temperature, and each regime can be characterized based on the corresponding dislocation behavior; (1) lattice resistance dominant; (2) segmentation dominant, and (3) steady-state segmentation. We will discuss the presence of these three regimes in terms of the temperature-dependence of lattice resistance and the dynamics of dislocation segmentation in the nano-scale volume. Note that our simulation results would not be applied only to Nb and Mo but can also be applied to other bcc metals. Thus, our results will provide a mechanistic description of the dislocation multiplication process of a screw dislocation in bcc metals at small length scales at various temperatures.

2. Methods

2.1. Basic simulation set-up

SCDM in bcc metal nanowires was systematically studied as a function of material and temperature. We chose bcc Nb and Mo due to their large difference in Peierls barrier (Nb: 70 MPa and Mo: 629 MPa [26] measured by bulk-scale experiments), which influences the mobility of screw dislocations. The range of temperature was appropriately chosen (10~400K for Nb and 10~800K for Mo) to study the transitions of SCDM processes. We did not study SCDM at too high temperatures because a significant thermally-activated events make the analysis of dislocation structure too difficult. Also, we do not discuss size effects in this study and focus only on how the temperature change influences SCDM processes at a given nanometer scale. Size effects will be presented in a separate publication.

The MD simulations were conducted using 'Large-scale Atomic/Molecular Massively Parallel Simulator' (LAMMPS) [27] under NσT ensemble time integration via Nose/Hoover method with Finnis-Sinclair (FS) potential for Mo [28] and Embedded-atom method (EAM) potential for Nb [29]. These interatomic potentials have been extensively used for various simulations, and their transferability has been demonstrated successfully. Both interatomic potentials were used reliably in MD simulations at temperatures and loading conditions used in our work [19, 30, 31]. The stresses were computed by using the constant NPT time integration via Nose/Hoover. In fact, the LAMMPS code provides the macroscopic stress tensor for the simulation cell volume. To obtain the stress tensor for our pillar, the LAMMPS stress tensor outputs must be scaled by the ratio of the pillar volume to the cell volume. This ratio is exactly the same with the ratio of the cross-sectional area of pillar to the top (or bottom) area of simulation cell because the height is identical.

To calculate the cross-sectional area of pillar, the diameter (D) of pillar was estimated by measuring the distance between most distantly separated two atoms on the top surface, and then, the cross-sectional area of pillar was obtained by $\pi D^2/4$. The same method was also used to compute the stress in silicon nanowire in the work done by Kang and Cai [32], and the description of stress estimation is available in their paper.

The diameter and height of the nanowires were ~14 nm and ~31 nm, respectively, for all simulations (**Figure 1(a)**). The number of atoms for Mo and Nb were 310,600 and 282,600, respectively. We used the periodic boundary condition along x, y and z directions, but because the empty space is available around a pillar, the periodic images along x and y directions do not affect the pillar in the simulation cell. The nanowires that have a pure screw dislocation with **b**=a/2[1 1 1] on the (0 1 $\bar{1}$) plane were constructed using MD++ [33]. The initial position of the screw dislocation was carefully chosen (1.6 nm from the center of nanowire) to provide enough time for dislocation multiplication under a reasonable stress value (Figure 1(b)). We kept the same initial position of the screw dislocation for all simulations. We did not try to start from a dislocation-free system as usually considered to study the mechanical behavior of nanowires because it is challenging to control the behavior of dislocations due to the stochastic nature of thermally-activated process of dislocation nucleation [34, 35]. In this case, multiple dislocations are often nucleated together at the first yield point. These dislocations sometimes interact with each other, and dislocation multiplication could result from dislocation interaction in addition to surface-induced cross-slip. They are also nucleated at different locations and at different stress levels depending on the initial atomic velocity distribution. Furthermore, the dislocation nucleation stress, which is usually close to the theoretical strength, is always higher than the critical stress of surface-controlled dislocation multiplication in our study. Once a screw dislocation is nucleated, it will

always self-multiply under load-control, or the load will drop significantly under displacement control. Thus, it is difficult to study the effect of stress on surface-controlled dislocation multiplication when a simulation starts from the dislocation-free state. Therefore, we preferred to use a straight screw dislocation as an initial condition, and it is much easier to control the applied stress systematically.

At a given temperature, a wide range of constant compressive stress (σ_{zz}) was applied along the [0 0 1]-direction until we observe SCDM. Then, the critical axial stress of SCDM was taken as the lowest stress, at which a dislocation self-multiplies. In our analysis, we used the resolved shear stress of a [1 1 1](1 $\bar{2}$ 1) slip system ($\tau_{[111](1\bar{2}1)}$) because cross-slipped dislocations usually stay in [1 1 1](1 $\bar{2}$ 1) and [1 1 1]($\bar{2}$ 1 1) slip systems, both of which have the same Schmid factor, 0.236 under the [0 0 1] loading. Note that at an elevated temperature, a single dislocation can sometimes reside on multiple slip planes due to localized cross-slip events, but we still used $\tau_{[111](1\bar{2}1)}$ for the consistent comparison. Dislocation structures were visualized based on the Dislocation Extraction Algorithm (DXA). Surface atoms and dislocation atoms were visualized by Ovito [36]

Additionally, to evaluate the effects of periodic image dislocations by changing the z-dimension of simulation cell, we also conducted the simulation with a nanowire three times longer in z-direction. However, we did not find any significant differences. This result implies that the effect of periodic image dislocations is less significant in determination of critical stress, and the applied stress on the dislocation in a simulation cell controls the dislocation multiplication dominantly.

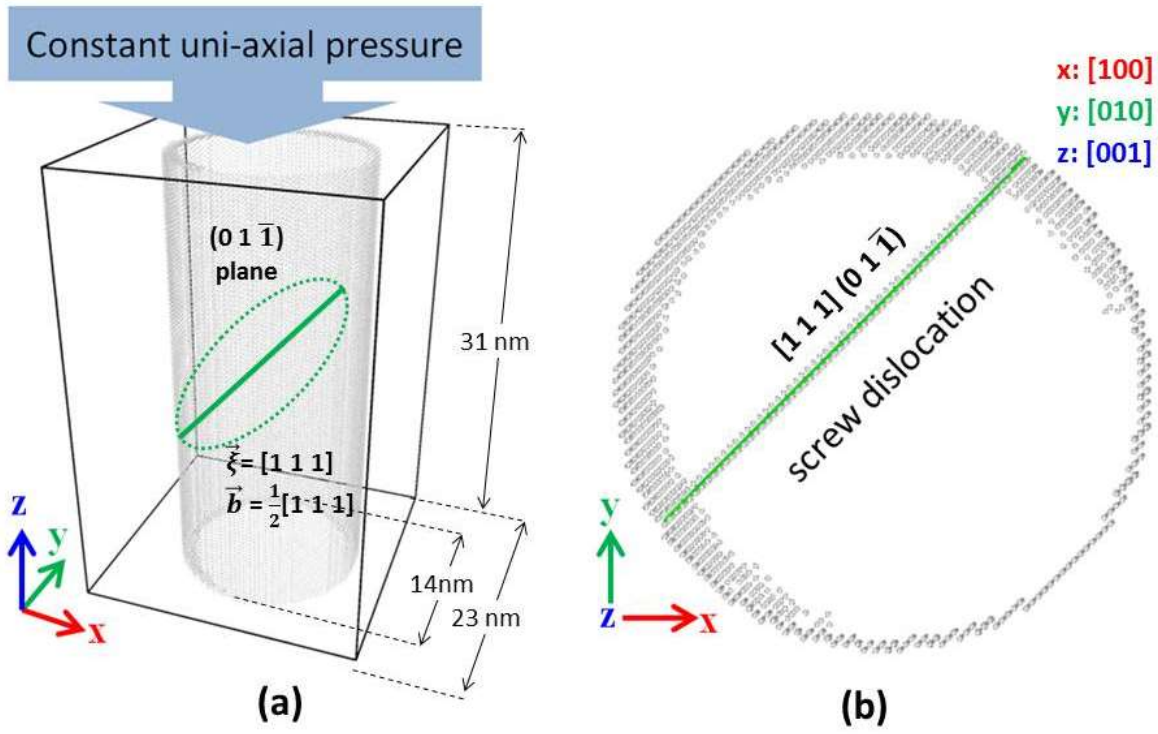

Figure 1. Initial atomistic simulation set-up (a) A nanowire containing a dislocation in a simulation box with periodic boundary condition in 3 dimensions; (b) The top view of a screw dislocation in a Nb nanowire.

2.2. Constant stress simulation

In this study, we do not use the low strain rate simulation. If the low strain rate is used, it is almost impossible to study the effect of stress because the applied stress changes over time and a dislocation structure would already change significantly before a target stress is reached. Our simulation aimed to observe how a screw dislocation behaves under a constant stress directly from the beginning of the simulation. In this way, it is possible to avoid any complications caused by the evolution of dislocation structure that occurs until a stress reaches the target stress.

To confirm the importance of constant stress application from the beginning of the simulation, we first tried the conventional method available in the default setting of LAMMPS. We increased the applied stress rapidly to the target stress and let the system stabilize toward the target stress state ($\sigma_{zz} \neq 0$ and $\sigma_{xx}=\sigma_{yy}=0$) as quickly as possible. We noted that σ_{zz} is easily stabilized, but the other two axial stresses (σ_{xx} and σ_{yy}) are not stabilized quickly. The sudden application of σ_{zz} at the beginning always induced significant elastic waves along the transverse directions. For instance, the initial application of σ_{zz} = 17.6 GPa produces a large transverse stress wave with the amplitude of σ_{xx} (σ_{yy}) = 5 GPa, which is nearly ~28% of σ_{zz} (**Figure 2**). These elastic fluctuations are diminished relatively slowly, thus they could significantly affect the evolution of the dislocation structure. Thus, to perform a reliable constant stress simulation, the transverse elastic fluctuation must be suppressed from the beginning of the simulation.

In order to minimize the transverse elastic fluctuations, we imposed axial pre-strains (ε_{xx}, ε_{yy}, and ε_{zz}). First, we estimated the required pre-strain values based on the anisotropic elasticity theory. Then, all atoms were displaced according to the calculated pre-strains. However, the elasticity calculation is not the optimized solution at every temperature used in this study. Thus, we systematically increased or decreased the lateral dimension until the transverse elastic fluctuation was almost completely suppressed. **Figure 2** shows the large difference in stress amplitude when the pillar dimension is pre-adjusted or not. Therefore, it is important to pre-adjust the dimensions of the nanowire to perform constant stress simulations properly. Within each simulation the amplitude of the transverse elastic waves was less than 0.5 GPa; this ensures that the effect on dislocation behavior is negligible.

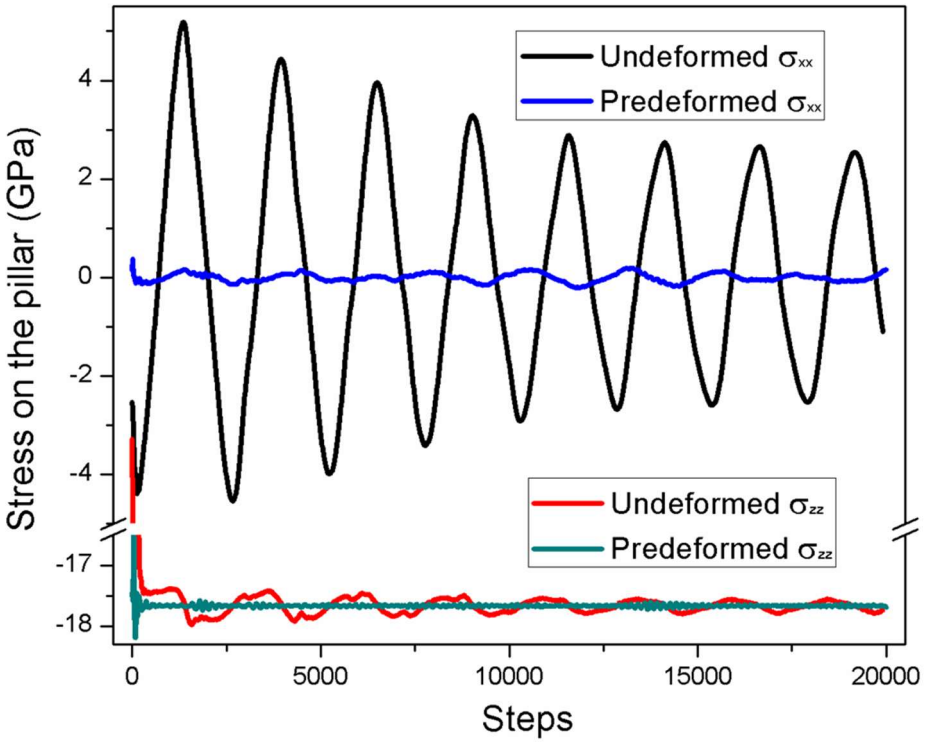

Figure 2. The effect of pre-strain on the transverse stresses. The application of pre-strain successfully suppresses the transverse elastic waves from the beginning of the simulation.

3. Results and Discussion

As described in Weinberger *et al.*'s work, if the applied stress is higher than the critical shear stress, a screw dislocation becomes the dynamic dislocation source, which produces new dislocations (**Figure 3**) [19]. In our study, following Weinberger *et al.*'s definition, the critical shear stress of SCDM was selected only when the isolated secondary dislocation is successfully formed and glides. Then, we obtained the critical shear stress leading to SCDM as a function of temperature. We confirmed that our room temperature data of Mo nanowires agrees with Weinberger *et al*.'s results based on their scaling relation (our nanowire is smaller than their smallest nanowires) [19]. This result ensures that our simulation was correctly set up. In this study, when different temperatures were considered, we found that there are three distinct regimes of critical shear stress of SCDM with respect to temperature in both Nb and Mo nanowires (**Figure 4**). The details of each regime will be discussed in the following sub-sections.

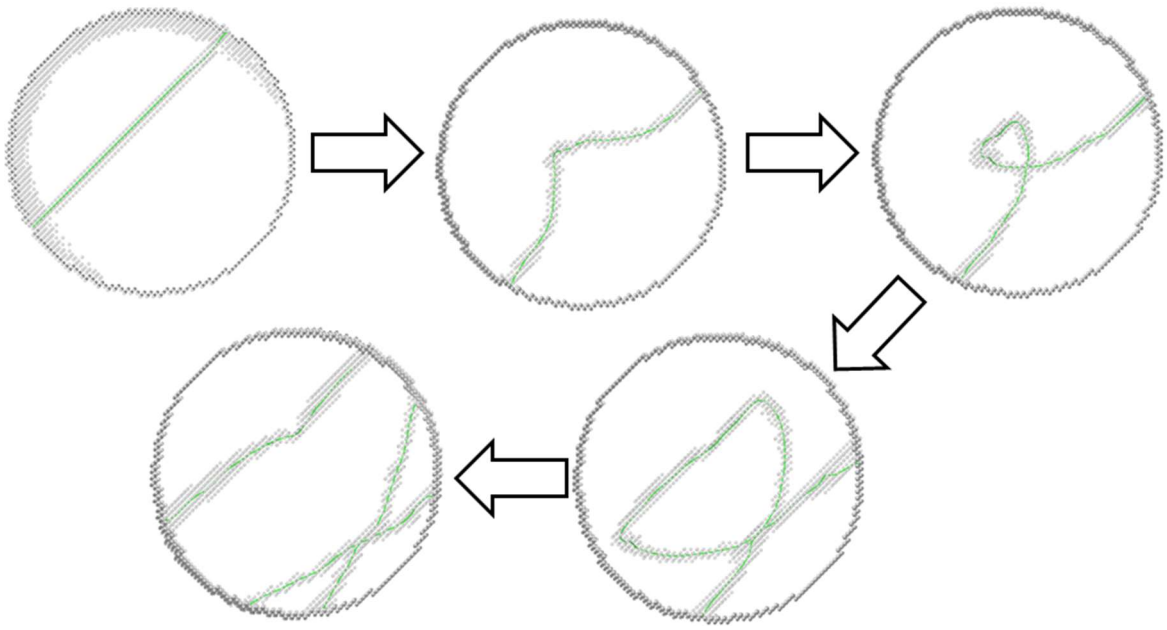

Figure. 3. Surface-controlled dislocation multiplication in a bcc Mo nanowire (T=10K, σ_{zz}=7.5 GPa). The multiplication process is consistent with Weinberger *et al.*'s results [19].

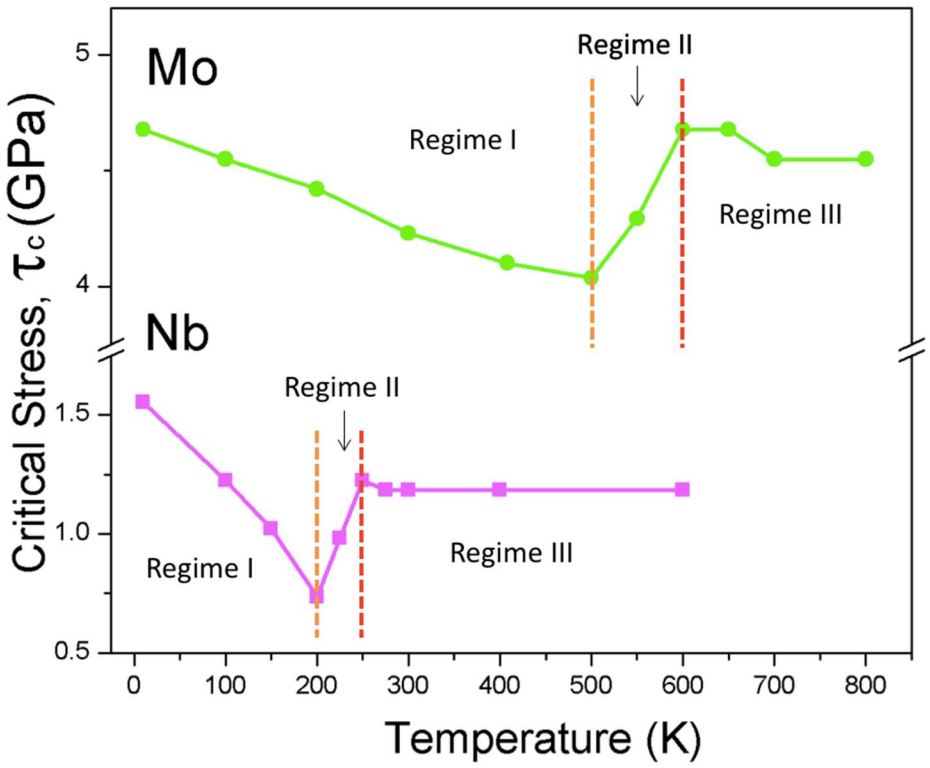

Figure. 4. Critical resolved shear stress ($\tau_{[111](1\bar{2}1)}$) as a function of temperature. There are three distinct regimes of critical shear stress of SCDM with temperature for both Nb and Mo nanowires. In Regime I, the critical shear stress decreases with temperature, but in Regime II, the critical shear stress increases abruptly. After the small peak value, the critical shear stress becomes nearly constant in Regime III.

3.1. Regime I: Lattice resistance control

In Regime I, the SCDM behavior resembles the behavior observed in Weinberger *et al.*'s Mo nanowire simulations done at room temperature, which belongs to Regime I according to our results (**Figure 4**). Cross-slip occurs at both ends of the dislocation due to the image stresses, and the screw dislocation moves onto [1 1 1](1 $\bar{2}$ 1) and [1 1 1]($\bar{2}$ 1 1) slip systems. Then, the cusp is

formed in the middle of the dislocation. If the applied stress is higher than a critical shear stress, the dislocation with the cusp produces the secondary dislocation (**Figure 3**). We noticed that in Regime I, the critical shear stress ($\tau_{[111](1\bar{2}1)}$) of SCDM decreases monotonically with temperature for both Nb and Mo nanowires (**Figure 4**). The critical shear stress of Mo nanowires is ~4.6 GPa at 10K and ~4.0 GPa at 500K, whereas that of Nb nanowires is ~1.6 GPa at 10K and is ~0.7 GPa at 200K.

The mobility of screw dislocations in bcc metals is usually a strong function of temperature and is determined by the nucleation and propagation of double kinks. The double-kink mechanism is a thermally-activated process [37, 38]. At higher temperatures, thus, the nucleation rate of double kinks becomes higher, leading to the higher mobility of a screw dislocation at a given stress. At early stages of simulations, we carefully monitored the motion of dislocation and confirmed that it moves faster at a higher temperature. For instance, at ~1.23 GPa, a screw dislocation in Nb nanowire barely moves at 10 K but moves much farther at 200 K (**Figure 5**). In case of Mo, the result looked similar (not shown here). At a given stress, therefore, a dislocation can move forward more easily at higher temperatures, leading to the lower critical shear stress of SCDM in Regime I.

The mobility of dislocation is usually related to the magnitude of intrinsic lattice resistance, which is the critical shear stress required for the motion of a straight and infinitely-long single dislocation without elastic interaction with other dislocations. Usually, the higher the intrinsic lattice resistance is, the lower the mobility of dislocation is. At any given temperature, the intrinsic lattice resistance of Mo is known to be higher than that of Nb [7, 26]. Thus, the higher critical shear stresses for SCDM in Mo nanowires within Regime I would result partly from its higher

intrinsic lattice resistance (**Figure 4**) (The contribution of dislocation line tension will be discussed in Section 3.4.).

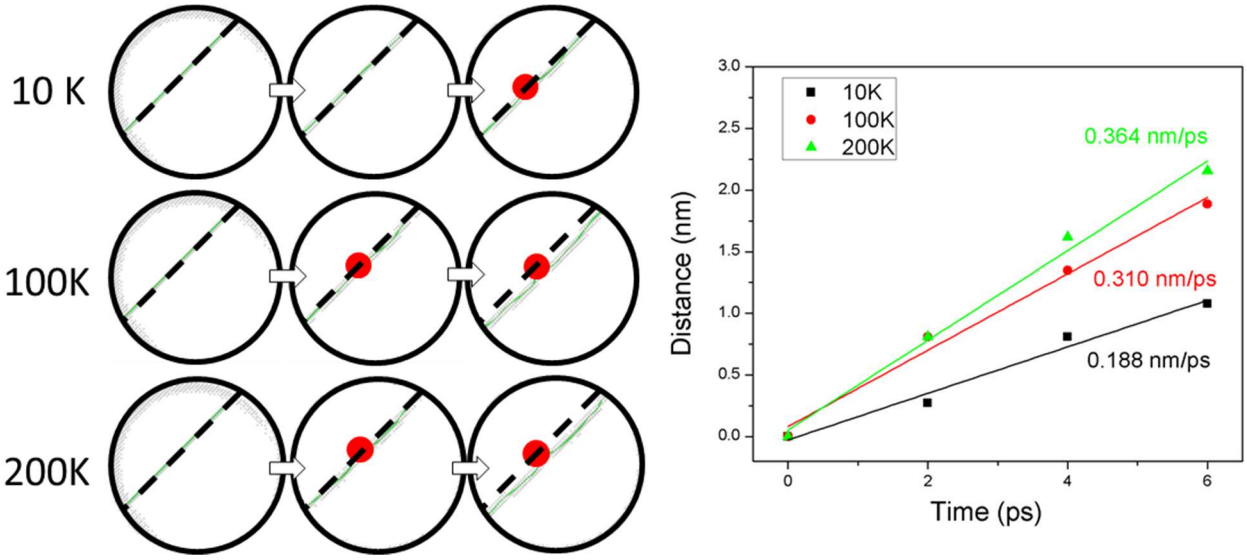

Figure 5. Temperature-d (a) nt dislocation motion in Regime I. (a) (b) ion motion at a given stress/time but at di.. .emperatures in Nb nanowire at 0, 2, 4 pi..s..nds. Dotted line indicates the initial position of dislocation. (b) The travel time-distance profile of surface node (red circle) along the [1 1 1] direction. The velocity component along the [1 1 1] direction was obtained by the linear fitting.

3.2. Regime II: Dynamic cross-slip dominant

As the temperature continues to rise from Regime I, the critical shear stress of SCDM stops decreasing and begins to increase abruptly (**Figure 4**). The critical shear stress of Mo nanowires increases up to 4.7 GPa for the shorter range of temperature from 500K to 600K. The critical shear stress of Nb nanowires increases up to 1.2 GPa over 50K range from 200 to 250K. These results are not consistent with the generally accepted idea of intrinsic lattice resistance discussed in

Section 3.1. Therefore, there might be the operation of another thermally-activated dislocation mechanism.

We carefully compared the evolution of dislocation structures in Regime II with that in Regime I. The evolution of the dislocation structure in Nb nanowires was monitored at the constant stress of 1.14 GPa and at 250 K (Regime II, no multiplication condition). At 250 K, we found that additional cross-slip occurs at the free surface, and the dislocation suddenly consists of three segments (**Figure 6**). Here, a segment means a section of dislocation that resides on the slip plane different from that of neighboring segments. We made a thin slice of sample, which is parallel to a slip plane to monitor the trajectory of the dislocation segments as a function of time and identified the slip plane of each segment precisely. For instance, in the case of Nb nanowires, a dislocation stays on the $(\bar{2}\ 1\ 1)$, $(1\ 1\ \bar{2})$, and $(1\ \bar{2}\ 1)$ planes in the middle of simulation. Note that the $(1\ 1\ \bar{2})$ slip plane was not observed in Regime I. The cross-slip events in Regime I were driven only by the image stress and was a completely athermal process (In other words, it can occur even at 0 K.) [19], but the additional cross-slip in Regime II could be a thermal process. Note that cross-slip is usually regarded as a thermal activation process. This thermally-activated cross-slip is less likely to occur at a low temperature (Regime I) but could occur easily at a higher temperatures (Regime II). In Regime II, therefore, the thermally-activated cross-slip could lead to the segmentation of dislocation.

If the temperature becomes higher, a thermal cross-slip event would occur more vibrantly, and the dislocation would be segmented more easily. The operation of Frank-Read type dislocation source is inversely proportional to the length of the dislocation source, which would correspond to the length of longest segment in our case. The critical shear stress of Frank-Read type dislocation source (τ_{F-R}) is usually expressed by $\mu b/L$, where μ is the shear modulus, b the magnitude of

Burgers vector, and L the source length. Obviously, the source length (L) becomes abruptly shorter once a dislocation is segmented and therefore the source operation stress (τ_{F-R}) could increase abruptly, too. Although the intrinsic lattice resistance keeps decreasing as the temperature increases, the dislocation segmentation would be much more dominant in the determination of the critical shear stress of SCDM in Regime II. This explains the sudden change in critical shear stress Regime II within the narrow temperature range.

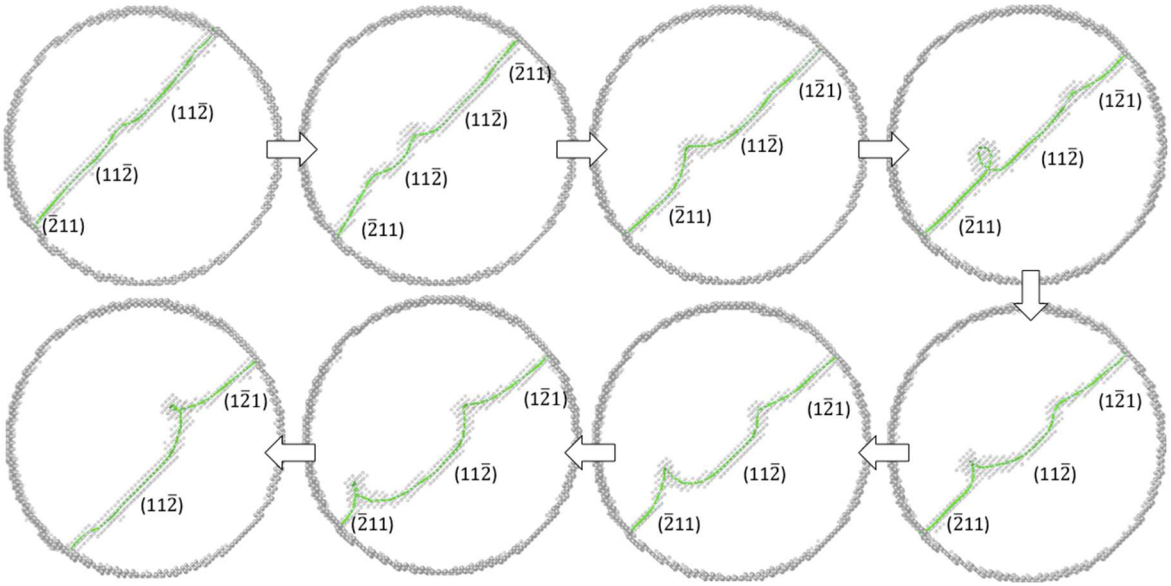

Figure 6. Evolution of dislocation structures in Regime II. Dislocation segmentation in Nb nanowire at τ=1.14 GPa and 250 K. Note that three dislocation segments are available in the middle of the simulation.

The similar self-pinning behavior was observed in Marian *et al.*'s MD simulation on a screw dislocation in bcc iron [39]. This work demonstrated that a line structure of dislocation becomes rough due to dynamic cross-slip events, leading to the more difficult motion of dislocation, called dislocation roughening. Dislocation roughening is the transition from a smooth

line of dislocation moving via formation and migration of atomic-sized kinks to a rugged line moving in a jerky way and leaving debris and vacancies behind. We also, sometimes, observed the formation of vacancies behind a dislocation in Regime II (**Figure 7**).

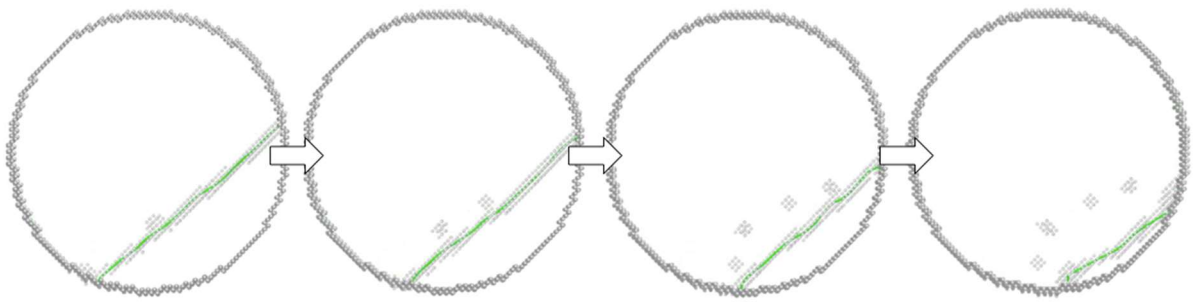

Figure 7. Formation of vacancies after the motion of dislocation in Regime II. Thermally-assisted evolution of dislocation structures produces vacancies.

3.3. Regime III: Segmentation Steady-state

As discussed in the previous two Sections, there are two competitive mechanisms in the operation of dynamic dislocation source; lattice resistance and dislocation segmentation. Our results show that the effect of these two main mechanisms becomes saturated in Regime III (**Figure 4**). The saturation of critical shear stress could be understood by the balance between the formation and annihilation of dislocation segments. Each segment is joined at the connecting node, i.e., pinning point, which is also mobile. We noticed that the source operation sometimes pushes out the connecting nodes toward the free surface, and the surface dislocation segment is annihilated. In Regime III, we often saw that the first connecting node is annihilated (**Figure 8**). Thus, at a temperature in Regime III, the creation of dislocation segment due to thermal cross-slip would balance with the annihilation at the free surface. Then, the total number of segment (or the average

length of each segment) would be relatively constant, and the critical shear stress of SCDM does not change much in Regime III. In Regime III, the intrinsic lattice resistance is zero for both Nb and Mo. Thus, the critical stress of SCDM would be determined by dislocation structure more than dislocation mobility. Because a dislocation structure is dynamically under steady-state, constant critical stress of SCDM can be expected as seen in our results (**Figure 4**).

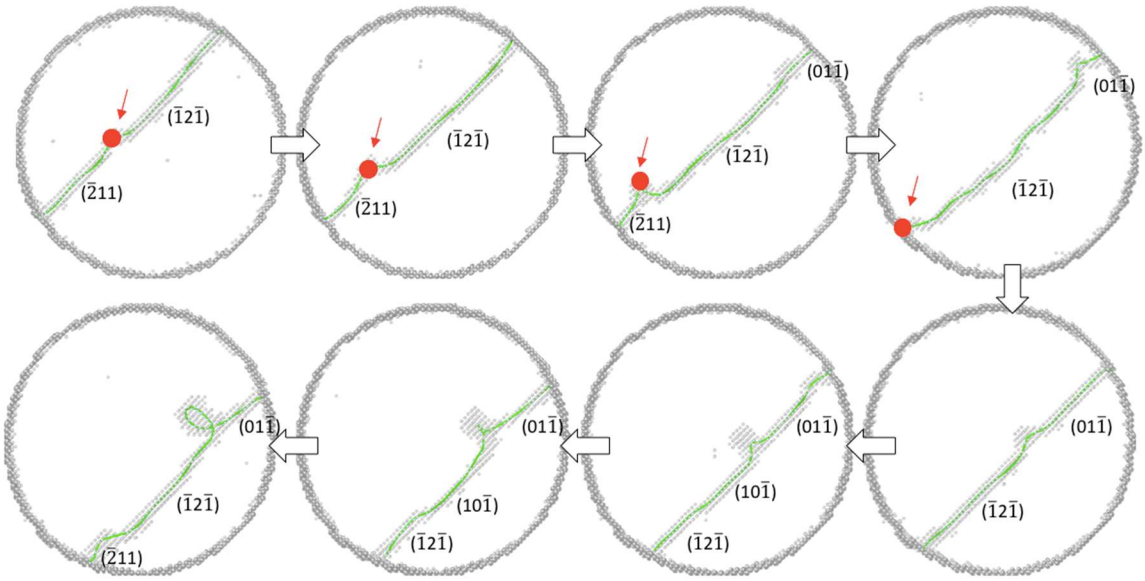

Figure 8. Evolution of dislocation structures in Regime III. In Regime III, dislocation segmentation becomes more dynamic, so cross-slip occurs more vibrantly. Creation and annihilation of dislocation nodes occur continuously. The red point (with the red arrow) corresponds to the dislocation node, which is initially created, and is annihilated during the motion of dislocation.

3.4. Dislocation source model

As Weinberger *et al.* suggested, the SCDM is fundamentally similar with the dislocation multiplication of Frank-Read source. Several micropillar studies have suggested that the operation of dislocation source at the nano-/micro-meter scale consists of three contributions, (1) intrinsic lattice resistance, (2) elastic interaction with other dislocations, and (3) dislocation line tension [40]. Because we have only one dislocation at the beginning of simulation, the elastic interaction term could be ignored. Thus, the intrinsic lattice resistance and dislocation line tension would be the major factors that determine the critical shear stress of SCDM.

Regime I shows the monotonic decrease in critical shear stress. As a first order approximation, let us assume the linear dependence of critical shear stress with temperature (**Figure 9(a)**). Because there is no segmentation in Regime I, the effects of line tension should be nearly constant in Regime I. In Regime II, the effect of line tension increases significantly due to the dislocation segmentation but becomes constant in Regime III. Thus, we can assume that the contribution of line tension to the critical shear stress for SCDM is nearly a step-like function (**Figure 9(b)**). Finally, the total three regimes can be described by the summation of the temperature-dependent lattice resistance and line tension (**Figure 9(c)**). Surprisingly, our model can capture even the presence of the small peak at the beginning of region III (**See the arrow in Figure 9(c)**). The combined effects of lattice resistance tail and segmentation saturation at the beginning of Regime III produces the small peak of critical shear stress. Once the lattice resistance becomes zero, the critical shear stress of SCDM becomes constant due to the steady-state segmentation as discussed in Section 3.3.

Based on the suggested scheme above, it is possible to extract the contributions of lattice resistance and line tension separately from our simulation results (**the second and third figures in Figure 9(b) and 9(c)**). First, based on our analysis above, we can assume that the lowest

temperature in the constant critical shear stress range in Regime III corresponds to the temperature at which the lattice resistance disappears completely. Then, we can estimate the temperature dependence of lattice resistance with the linear-fitted line that starts from the zero lattice resistance point. This fitted line of lattice resistance should have the same slope with the simulation data because the line tension is not dependent on temperature in Regime I. Then, by subtracting the lattice resistance from the total data, we can obtain the temperature-dependent line tension data. This simple model also allows us to obtain several useful quantities such as the lattice resistance at 0 K (Peierl's barrier), the temperature at which the lattice resistance becomes zero, and the athermal stress of source operation (Regime I). All these quantities are available in **Table 1**. Therefore, our model can capture the general trend of critical shear stress of SCDM with temperature by combining the temperature dependences of lattice resistance and line tension (dislocation segmentation). Several calculations of intrinsic lattice resistance indeed show the nearly linear dependence of temperature only except the tail region at a high temperature [41]. In our works, other factors (the presence of free surfaces, the shape of dislocations, and the dislocation line tension) seem to slightly change the shape of curve from linear-like exponential to linear ones. As noted in the previous paragraph, it is challenging to extract the non-linear behavior from the data in Figure 4 because the contributions of other factors cannot be quantified easily. However, the linear approximation would be good enough as the first order approximation because the temperature dependence could not be far from the linear dependence.

Note that Nb has a low Peierl's barrier while Mo has a relatively high Peierl's barrier. Regardless of a large difference in Peierl's barrier, both showed the similar trend. This result implies that our observation could be extended to other bcc metal nanowires. Thus, the SCDM

behavior could be controlled generally by the temperature-dependent lattice resistance and the dynamics of dislocation segmentation in bcc metal nanowires.

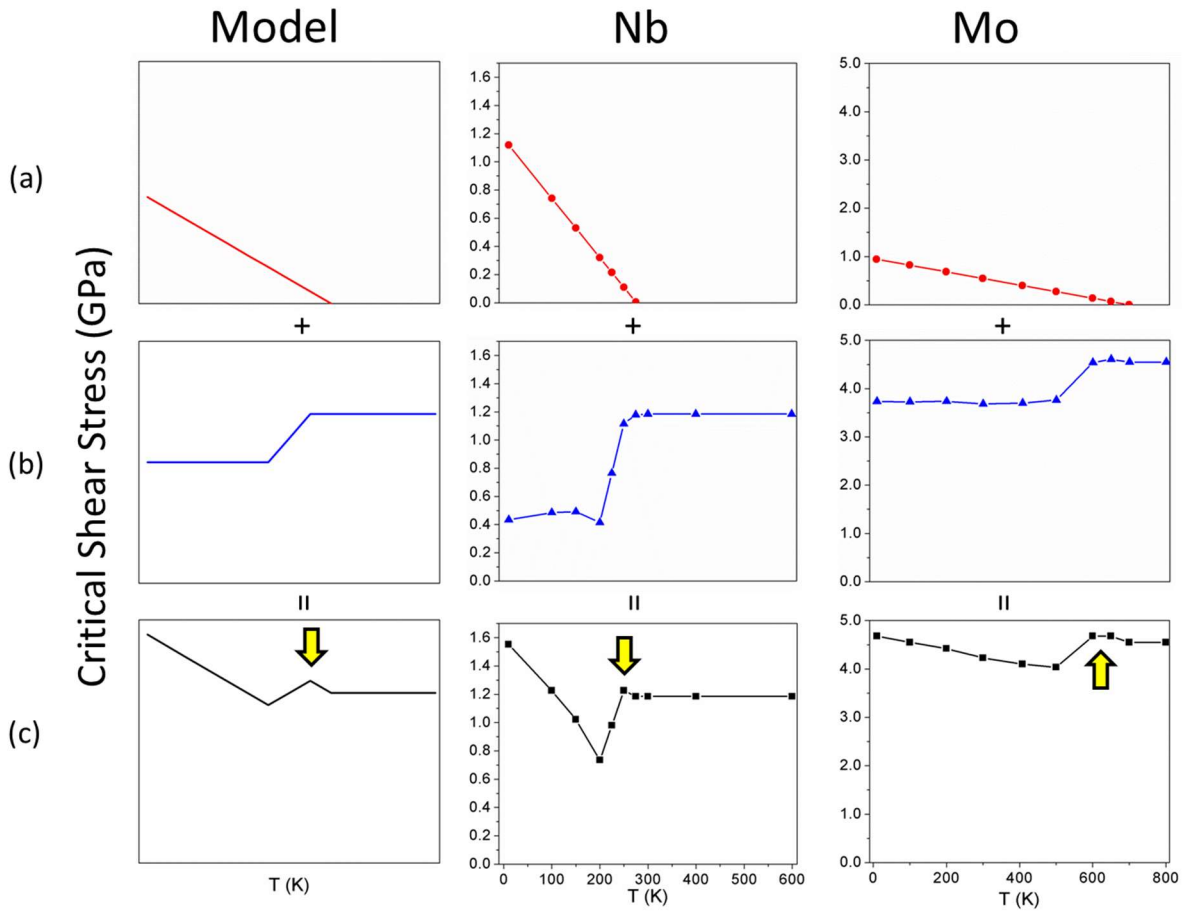

Figure 9. The effects of lattice resistance and line tension on the critical shear stress of SCDM. (a) Schematics of lattice resistance; (b) line tension; (c) the critical stress, which is the summation of (a) and (b). Starting from the left, the figures are from an analytic model, Nb nanowire simulations, and Mo nanowire simulations. Note that the tail of lattice resistance produces the small peak of critical shear stress at the beginning of Regime III. This result is consistent with our simulation data.

5. Concluding Remarks

The main goal of this work was to understand how temperature affects dislocation self-multiplication in bcc metals by means of atomistic simulations and a dislocation source model. We implemented the constant stress method to achieve more precise control of the applied stress. We observed that as temperature changes, the dislocation motion and its multiplication mechanism in both Nb and Mo nanowires appear to have three distinct regimes regardless of different lattice resistance (or Peierls barrier). Our analysis showed that the temperature dependence of lattice resistance and dislocation segmentation explain the presence of three different regime of critical shear stress. In Regime I, the lattice resistance varies with temperature, but there is no dislocation segmentation. Thus, the critical shear stress decreases with temperature in Regime I. In Regime II, dislocation segmentation starts to occur, so the line tension stress increases significantly. Thus, the critical shear stress abruptly increases with temperature in Regime II. In Regime III, the dislocation segmentation seems to be nearly constant, and the lattice resistance is completely removed. Thus, the critical shear stress does not change with temperature. In addition, we suggested a dislocation source model that combines the linear dependence of lattice resistance and the step function-like dependence of line tension stress. This model successfully describes three different regimes of critical stress and even the presence of a small peak at the early stage of Regime III. We believe that our results can provide a mechanistic description of the dislocation multiplication process of a screw dislocation in bcc metals at small length scales at various temperatures.

Acknowledgements

The work was supported by the grant (DE-SC0018895) funded by the U.S. Department of Energy, Office of Science. The authors gratefully acknowledge the financial support of UConn Start-Up Grant, the Storrs HPC cluster and the helpful advice of Garvit Agarwal and Professor Avinash M. Dongare.

Data availability

The raw/processed data required to reproduce these findings cannot be shared at this time as the data also forms part of an ongoing study.

References

[1] V. Volterra, in: Annales scientifiques de l'École normale supérieure, 1907, pp. 401-517.

[2] G.I. Taylor, Proceedings of the Royal Society of London. Series A, Containing Papers of a Mathematical and Physical Character, 145 (1934) 362-387.

[3] M.D. Uchic, D.M. Dimiduk, J.N. Florando, W.D. Nix, Science, 305 (2004) 986-989.

[4] D.S. Gianola, A. Sedlmayr, R. Mönig, C.A. Volkert, R.C. Major, E. Cyrankowski, S. Asif, O.L. Warren, O. Kraft, Review of Scientific Instruments, 82 (2011) 063901.

[5] S. Shim, H. Bei, M.K. Miller, G.M. Pharr, E.P. George, Acta Materialia, 57 (2009) 503-510.

[6] A. Budiman, S. Han, J. Greer, N. Tamura, J. Patel, W. Nix, Acta Materialia, 56 (2008) 602-608.

[7] Y. Cui, G. Po, N. Ghoniem, Acta Materialia, 108 (2016) 128-137.

[8] E.L. Huskins, Z.C. Cordero, C.A. Schuh, B.E. Schuster, Journal of materials science, 50 (2015) 7058-7063.

[9] S. Wang, Y. Yang, L. Zhou, Y.-W. Mai, Journal of Materials Science, 47 (2012) 6047-6055.

[10] Y. Yang, C.T. Liu, Journal of Materials Science, 47 (2012) 55-67.

[11] D. Dimiduk, M. Uchic, S. Rao, C. Woodward, T. Parthasarathy, Modelling and Simulation in Materials Science and Engineering, 15 (2007) 135.

[12] G. Song, T. Kong, K.J. Dusoe, P.C. Canfield, S.-W. Lee, Journal of Materials Science, 1-11.

[13] J.R. Greer, W.C. Oliver, W.D. Nix, Acta Materialia, 53 (2005) 1821-1830.

[14] S.-W. Lee, S.M. Han, W.D. Nix, Acta Materialia, 57 (2009) 4404-4415.

[15] K. Ng, A. Ngan, Scripta Materialia, 59 (2008) 796-799.

[16] H. Bei, S. Shim, E.P. George, M.K. Miller, E. Herbert, G.M. Pharr, Scripta Materialia, 57 (2007) 397-400.

[17] C. Chisholm, H. Bei, M. Lowry, J. Oh, S.S. Asif, O. Warren, Z. Shan, E.P. George, A.M. Minor, Acta Materialia, 60 (2012) 2258-2264.

[18] S. Brinckmann, J.-Y. Kim, J.R. Greer, Physical review letters, 100 (2008) 155502.

[19] C.R. Weinberger, W. Cai, Proceedings of the National Academy of Sciences, 105 (2008) 14304-14307.

[20] K. Maier, M. Peo, B. Saile, H. Schaefer, A. Seeger, Philosophical Magazine A, 40 (1979) 701-728.

[21] A. Misra, M. Demkowicz, X. Zhang, R. Hoagland, Jom, 59 (2007) 62-65.

[22] M. Brivio, W. Verboom, D.N. Reinhoudt, Lab on a Chip, 6 (2006) 329-344.

[23] I. Augustyniak, J. Dziuban, P. Knapkiewicz, M. Matusiak, M. Olszacki, P. Pons, in: Solid-State Sensors, Actuators and Microsystems (TRANSDUCERS & EUROSENSORS XXVII), 2013 Transducers & Eurosensors XXVII: The 17th International Conference on, IEEE, 2013, pp. 1503-1506.

[24] C.W. Roddy, R.L. Covington, K.M. Ravi, C. Bonavides, M. Bittar, G. Moake, B. Mandal, in, Google Patents, 2012.

[25] A. Schneider, D. Kaufmann, B. Clark, C. Frick, P. Gruber, R. Mönig, O. Kraft, E. Arzt, Physical review letters, 103 (2009) 105501.

[26] J. Millett, M. Cotton, N. Bourne, N. Park, G. Whiteman, Journal of Applied Physics, 115 (2014) 073506.

[27] S. Plimpton, Journal of computational physics, 117 (1995) 1-19.

[28] G. Ackland, R. Thetford, Philosophical Magazine A, 56 (1987) 15-30.

[29] M.R. Fellinger, H. Park, J.W. Wilkins, Physical Review B, 81 (2010) 144119.

[30] S. Kotrechko, O. Ovsjannikov, N. Stetsenko, I. Mikhailovskij, T. Mazilova, M. Starostenkov, Philosophical Magazine, 96 (2016) 473-485

[31] L.G. Wang, and A.Van de Walle, Physical Chemistry Chemical Physics, 14 (2012) 1529-1534.

[32] K. Kang, W. Cai, International Journal of Plasticity 26 (2010) 1387-1401.

[33] V. Bulatov, W. Cai, Computer simulations of dislocations, Oxford University Press on Demand, 2006.

[34] D. Mordehai, S-W. Lee, B. Backes, D.J. Srolovitz, W.D. Nix, E. Rabkin, Acta Materialia 59 (2011) 5202-5215.

[35] R. Kositski, O. Kovalenko, S-W. Lee, J.R. Greer, E. Rabkin, D. Mordehai, Scientific reports 6 (2016) 25966

[36] A. Stukowski, Modelling and Simulation in Materials Science and Engineering, 18 (2009) 015012.

[37] G. Po, Y. Cui, D. Rivera, D. Cereceda, T.D. Swinburne, J. Marian, N. Ghoniem, Acta Materialia, 119 (2016) 123-135.

[38] H. Conrad, W. Hayes, Trans. Am. Soc. Metals, 56 (1963).

[39] J. Marian, W. Cai, V.V. Bulatov, Nature Materials, 3 (2004) 158.

[40] B. Devincre, M. Condat, Acta metallurgica et materialia, 40 (1992) 2629-2637.

[41] T. Suzuki, H. Koizumi, H.O. Kirchner, Acta metallurgica et materialia 43 (1995) 2177-2187

Table 1. Useful quantities obtained by the dislocation source model

	Peierls barrier [GPa]	Temperature at which the lattice resistance becomes zero [K]	Athermal stress of source operation [GPa]
Mo nanowire	4.7	650	4.5
Nb nanowire	1.6	275	1.2